

**The following resources related to this article are available online at [www.sciencemag.org](http://www.sciencemag.org) (this information is current as of October 4, 2009 ):**

**Updated information and services**, including high-resolution figures, can be found in the online version of this article at:

<http://www.sciencemag.org/cgi/content/full/320/5881/1349>

**Supporting Online Material** can be found at:

<http://www.sciencemag.org/cgi/content/full/320/5881/1349/DC1>

A list of selected additional articles on the Science Web sites **related to this article** can be found at:

<http://www.sciencemag.org/cgi/content/full/320/5881/1349#related-content>

This article **cites 22 articles**, 9 of which can be accessed for free:

<http://www.sciencemag.org/cgi/content/full/320/5881/1349#otherarticles>

This article has been **cited by** 5 article(s) on the ISI Web of Science.

This article has been **cited by** 3 articles hosted by HighWire Press; see:

<http://www.sciencemag.org/cgi/content/full/320/5881/1349#otherarticles>

This article appears in the following **subject collections**:

Development

<http://www.sciencemag.org/cgi/collection/development>

Information about obtaining **reprints** of this article or about obtaining **permission to reproduce this article** in whole or in part can be found at:

<http://www.sciencemag.org/about/permissions.dtl>

lution of 5' boundaries because yeast 5' ends are often heterogeneous (9, 17) and we performed an amplification step. Instead, an approximate location was deduced by a sharp transition in signal over a small interval. Nonetheless, overall, RNA-Seq provides a useful map of exon boundaries. Our RNA-Seq method allowed us to map the transcriptional landscape of the yeast genome and define UTRs and previously unknown transcribed regions. In the future, application of this method should help to precisely determine the transcriptional landscape of other genomes.

#### References and Notes

- M. Snyder, M. Gerstein, *Science* **300**, 258 (2003).
- M. B. Gerstein *et al.*, *Genome Res.* **17**, 669 (2007).
- M. D. Adams *et al.*, *Nature* **377**, 3 (1995).
- P. Kapranov *et al.*, *Science* **296**, 916 (2002).
- P. Bertone *et al.*, *Science* **306**, 2242 (2004).
- Materials and methods are available as supporting material on *Science* Online.
- F. Perocchi, Z. Xu, S. Clauder-Munster, L. M. Steinmetz, *Nucleic Acids Res.* **35**, e128 (2007).
- L. David *et al.*, *Proc. Natl. Acad. Sci. U.S.A.* **103**, 5320 (2006).
- F. Miura *et al.*, *Proc. Natl. Acad. Sci. U.S.A.* **103**, 17846 (2006).
- M. Kellis, N. Patterson, M. Endrizzi, B. Birren, E. S. Lander, *Nature* **423**, 241 (2003).
- P. Cliften *et al.*, *Science* **301**, 71 (2003).
- K. Juneau, C. Palm, M. Miranda, R. W. Davis, *Proc. Natl. Acad. Sci. U.S.A.* **104**, 1522 (2007).
- F. Mignone, C. Gissi, S. Liuni, G. Pesole, *Genome Biol.* **3**, REVIEWS0004 (2002).
- A. G. Hinnebusch, *Annu. Rev. Microbiol.* **59**, 407 (2005).
- M. J. Ruiz-Echevarria, S. W. Peltz, *Cell* **101**, 741 (2000).
- F. C. Holstege *et al.*, *Cell* **95**, 717 (1998).
- C. F. Albright, R. W. Robbins, *J. Biol. Chem.* **265**, 7042 (1990).
- We thank S. P. Dinesh-Kumar for comments. Funded by two grants from NIH and one from the Connecticut Stem Cell Fund (P65CE01). The Gene Expression Omnibus accession number for sequences is GSE11209.

#### Supporting Online Material

www.sciencemag.org/cgi/content/full/1158441/DC1

Materials and Methods

Figs. S1 to S6

Tables S1 to S6

References

31 March 2008; accepted 22 April 2008

Published online 1 May 2008;

10.1126/science.1158441

Include this information when citing this paper.

# The Transcription/Migration Interface in Heart Precursors of *Ciona intestinalis*

Lionel Christiaen,<sup>1\*</sup> Brad Davidson,<sup>1†</sup> Takeshi Kawashima,<sup>2</sup> Weston Powell,<sup>1</sup> Hector Nolla,<sup>3</sup> Karen Vranizan,<sup>4</sup> Michael Levine<sup>1\*</sup>

Gene regulatory networks direct the progressive determination of cell fate during embryogenesis, but how they control cell behavior during morphogenesis remains largely elusive. Cell sorting, microarrays, and targeted molecular manipulations were used to analyze cardiac cell migration in the ascidian *Ciona intestinalis*. The heart network regulates genes involved in most cellular activities required for migration, including adhesion, cell polarity, and membrane protrusions. We demonstrated that fibroblast growth factor signaling and the forkhead transcription factor FoxF directly upregulate the small guanosine triphosphatase RhoDF, which synergizes with Cdc42 to contribute to the protrusive activity of migrating cells. Moreover, RhoDF induces membrane protrusions independently of other cellular activities required for migration. We propose that transcription regulation of specific effector genes determines the coordinated deployment of discrete cellular modules underlying migration.

There has been considerable progress in elucidating the gene regulatory networks controlling cell fate specification during animal development (1–3). In parallel, traditional in vitro assays coupled with more-recent proteome analyses have characterized the protein interaction networks controlling dynamic cellular processes, such as actin-based membrane protrusions (4) and adhesion (5). Comparatively little is known about how transient regulatory states interface with the dynamic cellular processes underlying morphogenesis. We investigated this problem using the migrating heart precursors of the ascidian *Ciona*

*intestinalis* as a relatively simple model. The ascidian heart develops from the B7.5 pair of blastomeres that specifically express the basic helix-loop-helix transcription factor Mesp in response to the T-box factor Tbx6 (6, 7). Subsequently, a fibroblast growth factor (FGF) signal activates the Ets1/2 transcription factor, a presumed Mesp target, and induces heart specification and cell migration of the anteriormost B7.5 granddaughter cells (Fig. 1A) (8). As a consequence, the heart precursors, called trunk ventral cells (TVCs), migrate into the trunk, whereas their sibling cells form anterior tail muscles (ATMs) (Fig. 1B). FGF signaling upregulates the forkhead box transcription factor FoxF in the TVCs. Interfering with FoxF function inhibits cell migration, but not heart muscle differentiation, showing that TVC migration is predominantly controlled by FGF signaling and the FoxF transcription factor (9).

To determine how FGF and FoxF control TVC migration, we developed a method for lineage-specific transcription profiling using fluorescence-activated cell sorting (FACS) and microarray analysis. The cis-regulatory DNAs from *Mesp* and the myogenic differentiation *MyoD* were used to express green and yellow fluorescent proteins in the

B7.5-lineage and surrounding mesodermal cells, respectively [Fig. 1B; Mesp, green fluorescent protein (GFP) transgenes; MyoD, yellow fluorescent protein (YFP) transgenes]. B7.5-lineage cells were sorted based on their GFP fluorescence, after targeted manipulations of Mesp, FoxF, and FGF signaling using the *Mesp* cis-regulatory DNA (Fig. 1, A to C) (7–9). Targeted expression of a dominant-negative FGF receptor (dnFGFR) converts the entire B7.5 lineage into ATMs (8) and is therefore expected to inhibit the expression of TVC-specific genes (Fig. 1A and fig. S3). In addition, modified versions of Mesp and FoxF (*Mesp*:VP16 and FoxF:WRPW, respectively; both are fusion proteins) block TVC migration but not cardiomyocyte differentiation (7, 9), thereby providing an opportunity to identify migration-specific genes (Fig. 1, A and E).

Microarray assays captured differential expression of known TVC- and tail muscle-specific marker genes (Fig. 1D and table S1). Moreover, at least 130 genes were found to be downregulated in all three conditions that inhibit TVC migration as compared with wild-type samples (Fig. 1E, fig. S4, and table S2). Transcriptional profiling of late gastrula stage B7.5 cells (LG sample) and whole tailbud embryos (whole sample) indicated that these 130 genes are upregulated in wild-type TVCs at the onset of migration (fig. S4). In situ hybridization assays validated the experimental design: 51 of 56 randomly selected candidate genes were expressed in migrating TVCs (Fig. 1, F and G, and fig. S3). Candidate migration genes include a broad spectrum of functional classes [for example, the RhoDF small Ras-homolog guanosine triphosphatase (Rho GTPase) and wunen-like phospholipid phosphohydrolase] (Fig. 1, F and G, and table S2). This diversity supports the view that many facets of cell migration are controlled transcriptionally (10, 11).

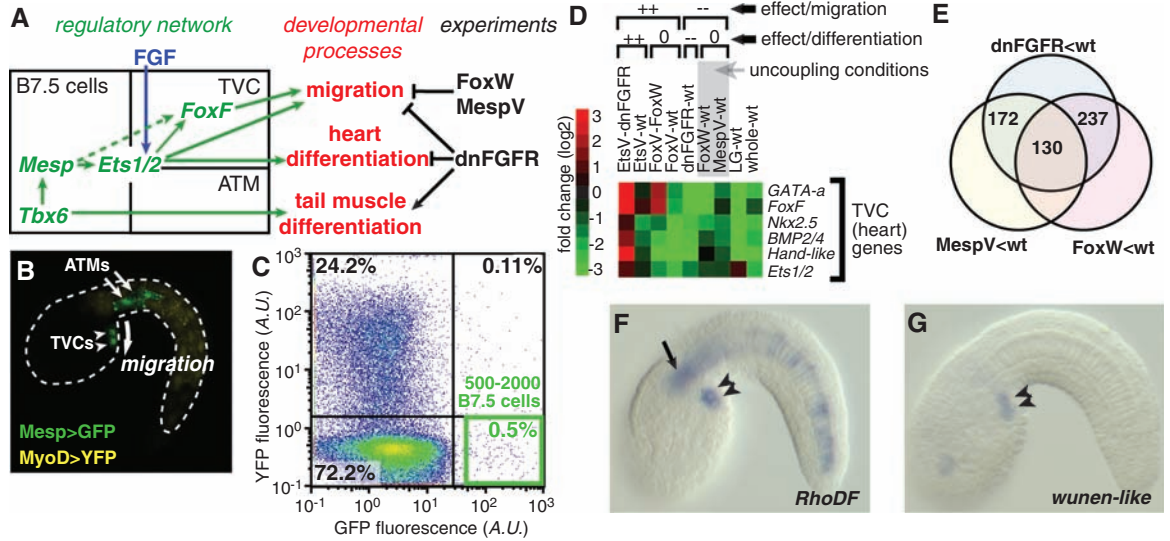
Specific gene families and biological processes have been implicated in directed cell migration, such as polarity, cell-matrix adhesion, and actin dynamics regulators (figs. S7 to S9). We compared the expression levels of individual genes in wild-type and dnFGFR samples, which permitted the identification of genes specifically upregulated in either TVCs or ATMs (Fig. 1A and figs. S5 and S9). Cell type-specific genes were found to func-

<sup>1</sup>Department of Molecular and Cell Biology, Division of Genetics, Genomics and Development, Center for Integrative Genomics, University of California, Berkeley, CA 94720, USA. <sup>2</sup>Department of Energy Joint Genome Institute, Walnut Creek, CA 94598, USA. <sup>3</sup>Cancer Research Laboratory, University of California, Berkeley, CA 94720, USA. <sup>4</sup>Functional Genomics Laboratory, University of California, Berkeley, CA 94720, USA.

\*To whom correspondence should be addressed. E-mail: lionelchristiaen@berkeley.edu (L.C.); mlewine@berkeley.edu (M.L.)

†Present address: Department of Molecular and Cellular Biology, Molecular Cardiovascular Research Program, University of Arizona, Tucson, AZ 85724, USA.

**Fig. 1.** Transcription profiling of heart precursors. (A) Regulatory network controlling developmental processes in the B7.5 lineage. Expression of dnFGFR, MespV, or FoxW inhibits cell migration. (B) Embryo expressing Mesp-GFP and MyoD-YFP transgenes. (C) FACS plot. Mesp-GFP<sup>−</sup> and MyoD-YFP<sup>−</sup> expressing cells are distinguished by their green or yellow fluorescence, respectively. The GFP-only quadrant (green box) was used to select B7.5-lineage cells. A.U., arbitrary units. (D) Experimental design and profiling of TVC marker genes. Effects on heart differentiation and cell migration are shown [for example, in column six FoxW inhibits migration (−), but not heart differentiation (0). Ets1/2:VP16, EtsV, and FoxF:VP16, FoxV have opposite effects from those of dnFGFR and FoxW, respectively; both enhance migration (++)]. wt, wild type. (E) Identification of 130 candidate migration



tion in each of the aforementioned cellular processes (figs. S7 to S9). For example, integrin-β3 and talin are upregulated in TVCs, possibly contributing to the changes in cell adhesion required for their migration. Conversely, ATM-specific up-regulation of myosin light-chain kinase (MLCK) and myosin regulatory light chain (MRLC) may enhance actomyosin contraction in tail muscles (fig. S9). Thus, the identified network may control most of the cellular processes underlying TVC and ATM morphogenesis.

Many components in the above pathways do not exhibit differential regulation in TVCs and ATMs, suggesting constitutive expression in the B7.5 lineage (Fig. 2A and figs. S6 to S9). For example, about two-thirds of the actin dynamics regulators are constitutively expressed in both cell types (fig. S8). *RhoDF* is the only Rho GTPase that is specifically upregulated in the TVCs (Fig. 2A and fig. S8). Taken together, these observations suggest that the heart network controls individual cellular processes by regulating subsets of effector genes.

Cell culture experiments demonstrated that the formation of membrane protrusions at the leading edge of migrating cells is powered by polarized actin polymerization (12, 13). In mammalian cells, both RhoD and RhoF/Rif were shown to directly activate the Diaphanous-related formin mDia2, which promotes the directed growth of actin filaments (14, 15). Our observations suggest that Mesp, FGF, and FoxF might control this process primarily through the transcriptional activation of *RhoDF* (Fig. 2A and fig. S9).

As a first step toward testing this model, we characterized *RhoDF* cis-regulatory sequences. A *RhoDF* lacZ fusion gene recapitulated endogenous *RhoDF* expression, including expression in TVCs and notochord cells, as well as inhibition by FoxF:WRPW (FoxW) (Fig. 2B and figs.

genes downregulated in conditions inhibiting cell migration as compared with wild-type samples (for example, dnFGFR<wt indicates genes showing reduced expression in dnFGFR as compared with wt samples). (F and G) In situ hybridization of selected candidate migration genes (*RhoDF* and *wunen-like*). Arrowheads indicate TVCs; arrow indicates *RhoDF* expression in the notochord.

genes downregulated in conditions inhibiting cell migration as compared with wild-type samples (for example, dnFGFR<wt indicates genes showing reduced expression in dnFGFR as compared with wt samples). (F and G) In situ hybridization of selected candidate migration genes (*RhoDF* and *wunen-like*). Arrowheads indicate TVCs; arrow indicates *RhoDF* expression in the notochord.

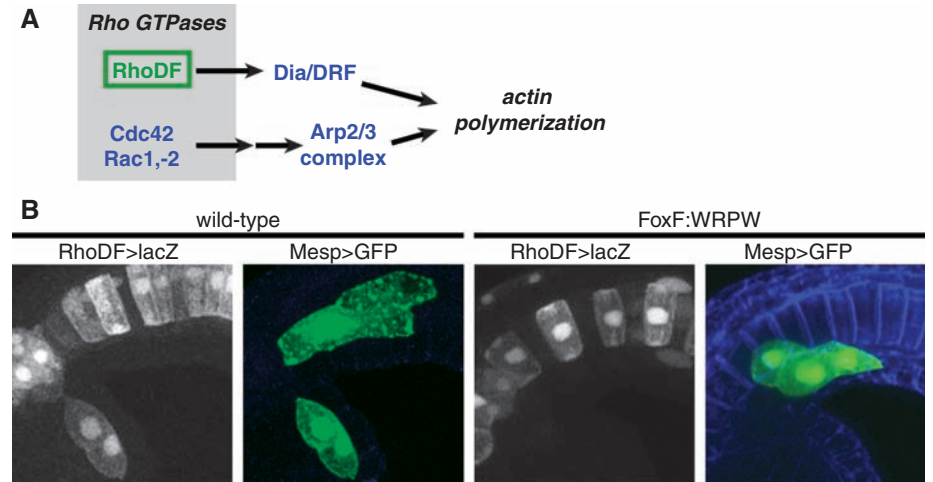


**Fig. 2.** The heart network regulates subsets of migration effectors. (A) Selected protein interactions promoting actin polymerization (extracted from fig. S9). Microarray analysis indicates that the Rho GTPase *RhoDF* is upregulated in the TVCs downstream of FGF and FoxF (green box and label). Diaphanous and Diaphanous-related formin (Dia/DRF); members of the Arp2/3 complex; and the Rho GTPases Rac1, Rac2, and Cdc42, are not differentially expressed between TVCs and ATMs (blue labels). Cdc42, Rac1, and Rac2 activate the Arp2/3 complex indirectly (successive arrows) (SOM text, section 6.4, and fig. S9). (B) *RhoDF*-lacZ (gray) expression in B7.5-lineage cells (marked by Mesp-GFP) is lost upon FoxF:WRPW coexpression. Blue indicates Alexa-phalloidin staining.

S10 and S11). Separate cis-regulatory modules control *RhoDF* expression in the notochord and TVCs (fig. S11). The minimal 425-base pair TVC enhancer contains putative Ets1/2- and FoxF-binding sites (fig. S11). Mutational analysis and cis-trans complementation assays demonstrated that both Ets1/2 and FoxF provide direct regulatory inputs for *RhoDF* upregulation in the TVCs (fig. S12). Therefore, FGF, FoxF, and *RhoDF* constitute a feed-forward circuit within the heart gene regulatory network.

The function of *RhoDF* in TVC migration was examined by injection of antisense morpholino

oligonucleotides (MOs) and targeted expression of dominant-negative (dn) and constitutively active (ca) mutants. MOs were coinjected with brachyury-GFP (16) and Mesp-GFP-moesin transgenes to visualize notochord cells and TVCs, respectively (Fig. 3A). Injection of a translation-blocking MO (ATG-MO) led to the formation of multicellular spheres (Fig. 3C). This severe phenotype presumably results from the inhibition of maternal mRNAs and suggests that *RhoDF* is essential for cell movements during early embryogenesis [supporting online material (SOM) text, section 8.2]. A splicing-inhibitor MO (E12) was used to inves-

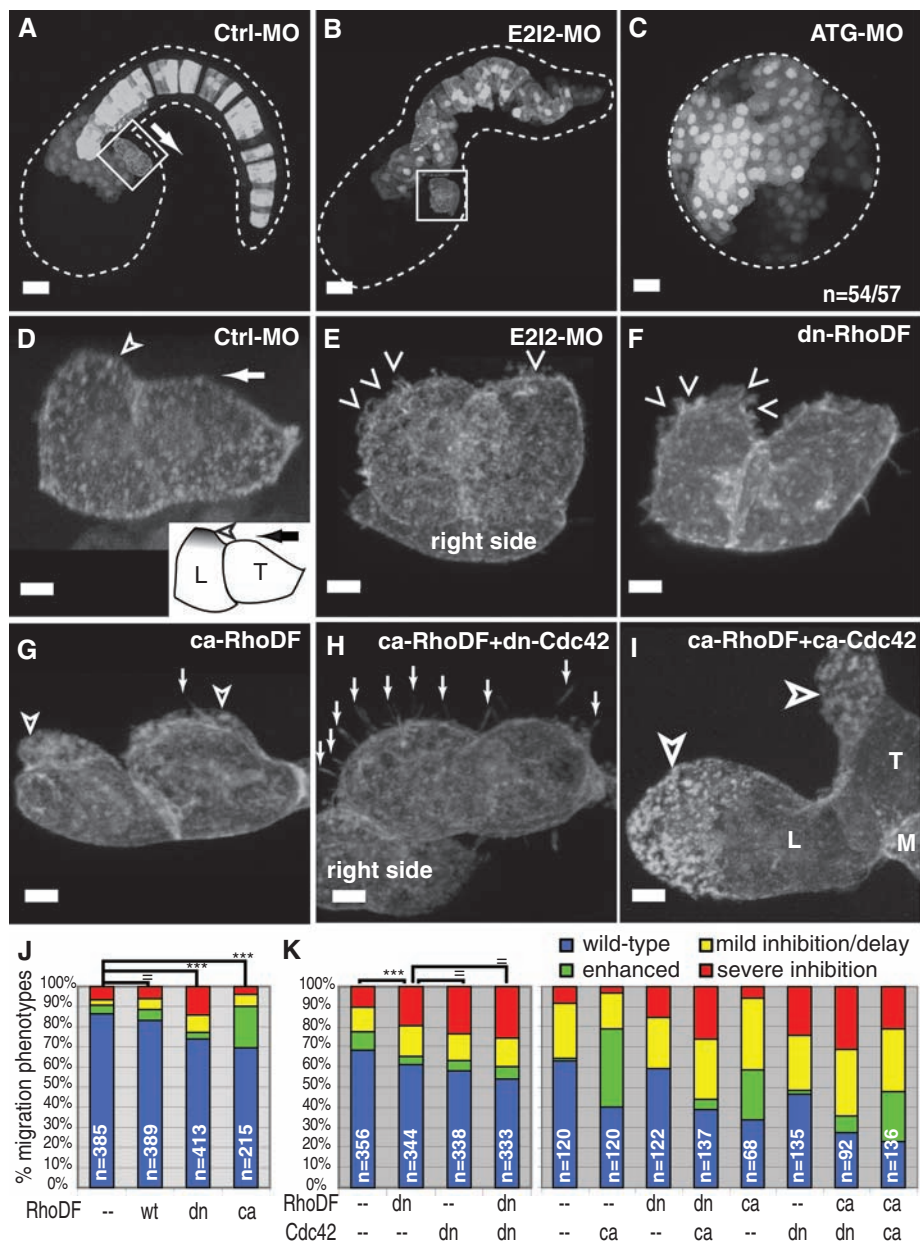


**Fig. 3.** RhoDF and Cdc42 synergy in TVC migration and protrusive activity. (A to C) Embryos injected with brachyury-GFP, Mesp-GFP-moesin, and indicated MOs. Scale bars, 20  $\mu$ m. (D and E) Magnified apical views of TVCs from (A) and (B). The arrows in (A) and (D) indicate the direction of migration. (F to I) TVCs expressing the indicated Rho GTPase mutants. Shown are apical views from three-dimensional projections (arrows, filopodia; solid arrowhead, lateral protrusion; open arrowheads, disrupted protrusion; L, leader; T, trailer; M, muscle cells;  $n > 10$  embryos for each condition. Scale bars, 5  $\mu$ m.). (J and K) Migration phenotypes. Histograms are from different pools of experiments ( $n$  is the number of B7.5 clusters scored. In  $\chi^2$  tests, for “=”  $P > 0.05$  and for “\*\*\*\*”  $P < 0.001$ .  $n > 3$  replicate experiments).

tigate the specific function of zygotic *RhoDF* transcripts (fig. S14). The E2I2 MO perturbed both TVC migration and notochord intercalation (Fig. 3B and fig. S14). Targeted expression of dn-RhoDF caused mild but statistically significant TVC migration defects, whereas ca-RhoDF appeared to enhance migration (Fig. 3J).

Detailed observations of the TVCs using an actin-binding GFP-moesin reporter (17) revealed that the leading cell (L) exhibits lateral protrusions enlarging its leading edge, whereas the trailing cell (T) is constricted at the trailing edge (Fig.

3D and fig. S13). Upon MO injection or dn-RhoDF expression, the cell contour was irregular and lateral protrusions appeared disrupted (Fig. 3, E and F). In contrast, ca-RhoDF induced a dramatic enlargement of lateral protrusions (Fig. 3G). Taken together, these observations suggest that RhoDF contributes to optimal TVC migration, possibly through the regulation of actin-based protrusions.

The ubiquitous Rho GTPase Cdc42, which also regulates actin-based protrusions, may function redundantly and/or in concert with RhoDF (18, 19). We investigated these possibilities by

coexpressing dn and ca forms of RhoDF and Cdc42 (Fig. 3, F to I and K, and fig. S15). dn-Cdc42 and dn-RhoDF produced similar migration and protrusion phenotypes, whether expressed separately or together, suggesting that they function synergistically in TVCs (Fig. 3, F and K, and fig. S15). ca-Cdc42 induced actin-rich protrusions that failed to extend upon coexpression of dn-RhoDF (fig. S15). More strikingly, dn-Cdc42 reduced the width of the ca-RhoDF-induced protrusions, often causing the formation of multiple filopodia (Fig. 3H). Finally, ca-RhoDF and ca-Cdc42 coexpression disrupted the TVCs’ polarity and produced protrusions that often covered the entire leading edge (Fig. 3I and fig. S15).

The simplest interpretation is that Cdc42 promotes actin-filament branching through indirect activation of the actin-related protein 2/3 (Arp2/3) complex (20, 21), whereas RhoDF induces actin filament elongation through the activation of Diaphanous-related formins (Fig. 2A). The precise balance of microfilament branching and elongation would then pattern the actin meshwork underlying membrane protrusion [Fig. 4B, fig. S15F, and (13)].

The preceding results suggest that upregulation of *RhoDF* by FGF and FoxF is sufficient to promote actin-based protrusions in TVCs because *RhoDF* works in concert with Cdc42 and other constitutive activators of actin polymerization (Fig. 2A). Additional epistasis assays were performed to determine whether RhoDF is indeed the only missing factor. Targeted expression of FoxF:WRPW, dnFGFR, or Ets:WRPW [a constitutive repressor form of Ets1/2 (8)] consistently blocked migration and the formation of lateral protrusions (Fig. 4A and fig. S16). Both wild-type and activated forms of RhoDF were sufficient to induce lateral protrusions in nonmigrating B7.5 cells expressing FoxF:WRPW (Fig. 4A and fig. S16). Cells coexpressing Ets:WRPW and ca-RhoDF formed smaller protrusions and filopodia, whereas dnFGFR eliminated the ability of ca-RhoDF to induce protrusions (fig. S16). These observations indicate that FGF signaling provides as-yet-unidentified inputs required for RhoDF/Cdc42-induced protrusive activity (Fig. 4B and fig. S16). The formation of RhoDF-induced protrusions in the FoxF:WRPW background indicates that FoxF controls membrane protrusion essentially through *RhoDF* upregulation and shows that protrusive activity is separable from other processes required for migration.

Our results illuminate previously unrecognized characteristics of the transcription/cell behavior interface. The heart gene network impinges on most of the individual cellular processes required for migration by regulating subsets of effector genes that function together with constitutively expressed proteins. These shared regulatory inputs probably contribute to the coordination of different cellular processes, which could nevertheless be uncoupled from one another, thus highlighting the intrinsically modular nature of cell behavior.

TVC-specific expression of *RhoDF* depends on FGF, Ets1/2, FoxF, and as-yet-unidentified

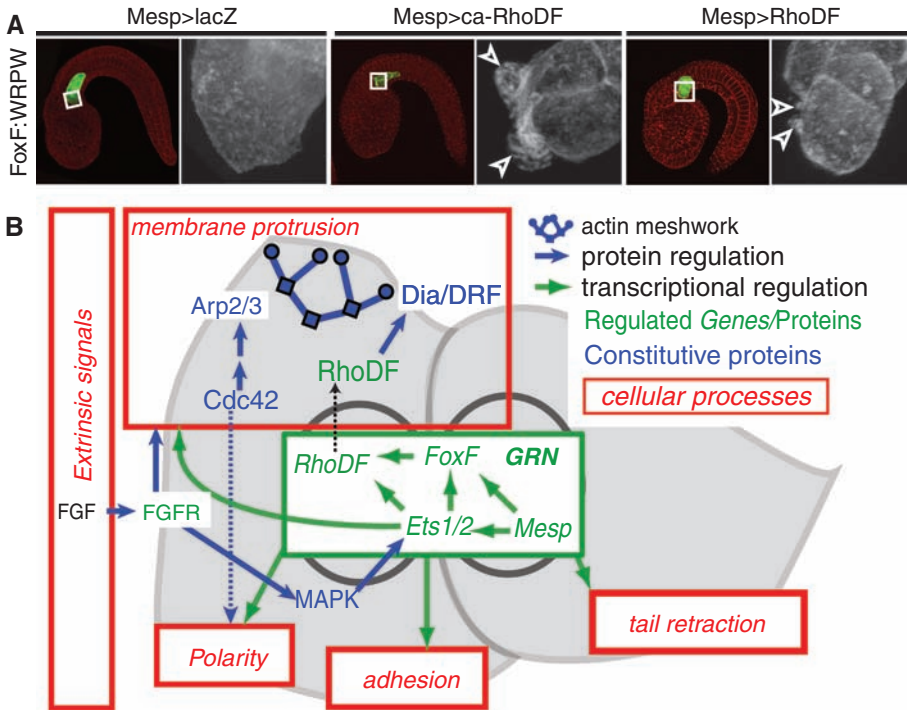


**Fig. 4.** RhoDF induces membrane protrusion in nonmigrating cells. **(A)** B7.5-lineage cells coexpressing FoxF:WRPW and lacZ, ca-RhoDF, or RhoDF. [Whole embryos and close-up views (boxes) are shown. Red indicates Alexa-phalloidin counterstaining.] Arrowheads indicate protrusions. **(B)** Summary model. The gene regulatory network (GRN) influences polarity, adhesion, tail retraction, and membrane protrusion. Membrane protrusion is controlled in part by FoxF- and Ets1/2-mediated upregulation of RhoDF, which functions together with constitutively expressed Cdc42, Dia/DRF (blue circles), and Arp2/3 (blue squares).

inputs, stressing the fact that RhoDF-induced protrusive activity is regulated by multiple inputs from the heart specification network (Fig. 4B and figs. S10 to S12). A separate enhancer controls *RhoDF* expression in the notochord (fig. S11). In principle, this modular organization of the *RhoDF* cis-regulatory elements permits activation by distinct gene regulatory networks in the notochord and TVCs. RhoDF contributes to the formation of protrusions in migrating TVCs and probably also in intercalating notochord cells (Fig. 3B and fig. S14). Unlike TVCs, notochord cells maintain adhesive contacts with their neighbors. In *laminin- $\alpha$ 3/4/5* mutants, these adhesive contacts are disrupted and notochord cells migrate away from their normal location, displaying dynamic protrusions reminiscent of those induced by ca-RhoDF (22) (fig. S15). Thus, the notochord and TVCs deploy different suites of shared (such as protrusions) and tissue-specific (such as adhesive properties) cellular modules. We propose that tissue-specific gene networks control the distinct combinations of cellular modules underlying the morphogenetic diversity observed during evolution and development.

**References and Notes**

1. A. Stathopoulos, M. Levine, *Dev. Cell* **9**, 449 (2005).
2. E. H. Davidson *et al.*, *Science* **295**, 1669 (2002).
3. K. S. Imai, M. Levine, N. Satoh, Y. Satou, *Science* **312**, 1183 (2006).
4. C. Bakal, J. Aach, G. Church, N. Perrimon, *Science* **316**, 1753 (2007).

5. R. Zaidel-Bar, S. Itzkovitz, A. Ma'ayan, R. Iyengar, B. Geiger, *Nat. Cell Biol.* **9**, 858 (2007).
6. Y. Satou, K. S. Imai, N. Satoh, *Development* **131**, 2533 (2004).
7. B. Davidson, W. Shi, M. Levine, *Development* **132**, 4811 (2005).

8. B. Davidson, W. Shi, J. Beh, L. Christiaen, M. Levine, *Genes Dev.* **20**, 2728 (2006).
9. J. Beh, W. Shi, M. Levine, B. Davidson, L. Christiaen, *Development* **134**, 3297 (2007).
10. L. Borghese *et al.*, *Dev. Cell* **10**, 497 (2006).
11. X. Wang *et al.*, *Dev. Cell* **10**, 117 (2006).
12. S. A. Koestler, S. Auinger, M. Vinzenz, K. Rottner, J. V. Small, *Nat. Cell Biol.* **10**, 306 (2008).
13. C. Yang *et al.*, *PLoS Biol.* **5**, e317 (2007).
14. P. A. Randazzo, *Dev. Cell* **4**, 287 (2003).
15. S. Pellegrin, H. Mellor, *Curr. Biol.* **15**, 129 (2005).
16. J. C. Corbo, M. Levine, R. W. Zeller, *Development* **124**, 589 (1997).
17. K. A. Edwards, M. Demsky, R. A. Montague, N. Weymouth, D. P. Kiehart, *Dev. Biol.* **191**, 103 (1997).
18. S. Ellis, H. Mellor, *Curr. Biol.* **10**, 1387 (2000).
19. C. D. Nobes, A. Hall, *Cell* **81**, 53 (1995).
20. R. Rohatgi *et al.*, *Cell* **97**, 221 (1999).
21. L. Ma, R. Rohatgi, M. W. Kirschner, *Proc. Natl. Acad. Sci. U.S.A.* **95**, 15362 (1998).
22. M. T. Veeman *et al.*, *Development* **135**, 33 (2007).
23. Microarray data available at ArrayExpress; accession number, E-MEXP-1478. We thank J. Beh, A. Philips, and P. Lemaire for sharing constructs; M. Blanchette and V. Peng for help with microarrays; Y. Satou for expressed sequence tag sequences and annotations; and W. Shi, K. Imai, and U. Rothbacher for help with microinjections. Authors' contributions were as follows: L.C. designed the project, performed and analyzed experiments, and prepared the figures; B.D. and T.K. designed the custom microarray; L.C. and W.P. performed in situ hybridizations; L.C. and H.N. performed the FACS experiments; L.C. and K.V. analyzed the microarray data; and L.C. and M.L. wrote the paper. This work was funded by NSF grant IOB 0445470 and NIH grant 18B-106681 to M.L., a grant from the Gordon and Betty Moore Foundation to the Center for Integrative Genomics, and an American Heart Association fellowship (0625042Y) to B.D.

**Supporting Online Material**

www.sciencemag.org/cgi/content/full/320/5881/1349/DC1  
 Materials and Methods  
 SOM Text  
 Figs. S1 to S16  
 Tables S1 and S2  
 References  
 21 March 2008; accepted 9 May 2008  
 10.1126/science.1158170

# High Impulsivity Predicts the Switch to Compulsive Cocaine-Taking

David Belin,<sup>1\*</sup> Adam C. Mar,<sup>1</sup> Jeffrey W. Dalley,<sup>1,2</sup> Trevor W. Robbins,<sup>1</sup> Barry J. Everitt<sup>1\*</sup>

Both impulsivity and novelty-seeking have been suggested to be behavioral markers of the propensity to take addictive drugs. However, their relevance for the vulnerability to compulsively seek and take drugs, which is a hallmark feature of addiction, is unknown. We report here that, whereas high reactivity to novelty predicts the propensity to initiate cocaine self-administration, high impulsivity predicts the development of addiction-like behavior in rats, including persistent or compulsive drug-taking in the face of aversive outcomes. This study shows experimental evidence that a shift from impulsivity to compulsivity occurs during the development of addictive behavior, which provides insights into the genesis and neural mechanisms of drug addiction.

Compulsive cocaine use has been hypothesized to result from a failure in top-down executive control over maladaptive habit learning (1, 2). In neural terms, this may reflect the diminishing influence of prefrontal cortical function, as behavioral control devolves from ventral to dorsal striatum (1). In behavioral terms, we predict that the development of addiction reflects a shift from impulsivity to compulsivity (3).

Human studies have implicated individual differences in different forms of impulsivity and sensation-seeking in vulnerability to drug use and abuse (4–6). However, whether the enhanced impulsivity observed in drug addicts (7, 8) predates the onset of compulsive drug use or is a consequence of protracted exposure to drugs has not been fully established. In addressing this issue experimentally, we operationalized these human traits in